© 2021. Published by The Company of Biologists Ltd | Journal of Experimental Biology (2021) 224, jeb235481. doi:10.1242/jeb.235481

RESEARCH ARTICLE

Intersection of motor volumes predicts the outcome of ambush predation of larval zebrafish

Kiran Bhattacharyya[1], David L. McLean[2] and Malcolm A. MacIver[1,2,3,*]

ABSTRACT

Escape maneuvers are key determinants of animal survival and are under intense selection pressure. A number of escape maneuver parameters contribute to survival, including response latency, escape speed and direction. However, the relative importance of these parameters is context dependent, suggesting that interactions between parameters and predatory context determine the likelihood of escape success. To better understand how escape maneuver parameters interact and contribute to survival, we analyzed the responses of larval zebrafish (*Danio rerio*) to the attacks of dragonfly nymphs (*Sympetrum vicinum*). We found that no single parameter explains the outcome. Instead, the relative intersection of the swept volume of the nymph's grasping organs with the volume containing all possible escape trajectories of the fish is the strongest predictor of escape success. In cases where the prey's motor volume exceeds that of the predator, the prey survives. By analyzing the intersection of these volumes, we compute the survival benefit of recruiting the Mauthner cell, a neuron in anamniotes devoted to producing escapes. We discuss how the intersection of motor volume approach provides a framework that unifies the influence of many escape maneuver parameters on the likelihood of survival.

KEY WORDS: Ambush, Escape, Predation

INTRODUCTION

An escalating arms race between predators and prey is a major driving force behind the evolution of diverse body plans (Sperling et al., 2013) and the nervous systems controlling them (Sillar et al., 2016). For prey, there is a selective benefit for those parameters of escape maneuvers and the underlying neural circuitry that lower their chances of being attacked and consumed (Sillar et al., 2016). It is known that the response latency, speed, and direction of an escape maneuver all contribute to a successful outcome for potential prey (Howland, 1974; Dangles et al., 2006; Stewart et al., 2013).

However, there are also examples where individual parameters are not as predictive of outcome. For example, successful escapes can be initiated at extremely short latency using large-diameter command neurons or in the absence of them (Edwards et al., 1999; Korn and Faber, 2005; Card, 2012; Hecker et al., 2020). Similarly, other results have both disputed and supported the utility of fast speeds for increasing evasion success (DiDomenico et al., 1988; DiDomenico and Eaton, 1988; Eaton et al., 1995; Webb, 1986; Katzir, 1993; Walker et al., 2005; Fuiman et al., 2006; Soto et al., 2015; Nair et al., 2017). Moreover, in some cases it is helpful to move in a specific direction to increase survival (Weihs and Webb, 1984; Eaton et al., 1991; Domenici, 2002), while in others it helps to be unpredictable and vary escape direction (Driver and Humphries, 1970; Edut and Eilam, 2004; Domenici et al., 2011a,b). Previous studies have argued that these differing results are due to the context-dependent importance of escape maneuver parameters (Domenici, 2010; Domenici et al., 2011a,b). This suggests that, beyond the influence of any single parameter, the interaction between parameters and predation context is critical in determining the likelihood of escape success. However, it is unclear how escape maneuver parameters interact with each other in various predatory contexts to contribute to escape success.

To better understand the determinants of successful escapes, we have studied the predation of larval zebrafish (*Danio rerio*), a popular model system for linking neural circuits to escape behaviors (Hale et al., 2016), by an ambush predator, the dragonfly nymph (*Sympetrum vicinum*). As a caveat, Asian dragonfly nymphs normally feed on *Danio* fish larvae (Engeszer et al., 2007) and *Sympetrum* nymphs normally feed on North American fish larvae, so the predator–prey context is relevant, if not strictly accurate. Dragonfly nymphs hunt by remaining motionless and waiting for prey to come within ambush distance (Robert Evans Snodgrass, 1954; Pritchard, 1965) (Fig. 1). Once in range, the nymphs attack prey with their hydraulically-powered prehensile masks (Olesen, 1972; Tanaka and Hisada, 1980; Parry, 1983; Busse and Gorb, 2018), which extend outward to grasp the prey with palps, confining them in a spoon-shaped bowl (Olesen, 1978; Blanke et al., 2015), hereafter referred to as the mask.

The study of ambush predation simplifies assessments of escape maneuver parameters compared with pursuit predation, exemplified by adult dragonflies (Mischiati et al. 2015; Lin and Leonardo, 2017), where it is more difficult to determine which parameter in a series of movements ultimately led to successful escape. In contrast, ambush predation, which involves sudden strikes by predators on unsuspecting prey (deVries et al., 2012), does not provide time for a series of movements. Consequently, we focused on single escape responses of larval fish to the ballistic strikes of dragonfly nymphs to find the parameters most predictive of the outcome.

Using our analysis of the kinematics of predator–prey encounters, we created a model of the mask motor volume – the volume swept by the grasping appendage over a given amount of time – and the fish motor volume – the volume containing all possible trajectories of the fish within the time remaining until mask arrival (Snyder et al., 2007). Using the model, we demonstrated that the fluid perturbations caused by the extending mask modulate the timing and kinematics of the fish escape response. We also use the model to estimate the survival benefit of recruiting the Mauthner cell, the giant neuron devoted to producing escape maneuvers in fish

[1]Department of Biomedical Engineering, Northwestern University, Evaxnston, IL 60201, USA. [2]Department of Neurobiology, Northwestern University, Evanston, IL 60201, USA. [3]Department of Mechanical Engineering, Northwestern University, Evanston, IL 60201, USA.

*Author for correspondence (maciver@northwestern.edu)

M.A.M., 0000-0002-3711-8235

Received 13 August 2020; Accepted 23 December 2020

Journal of Experimental Biology (2021) 224, jeb235481. doi:10.1242/jeb.235481

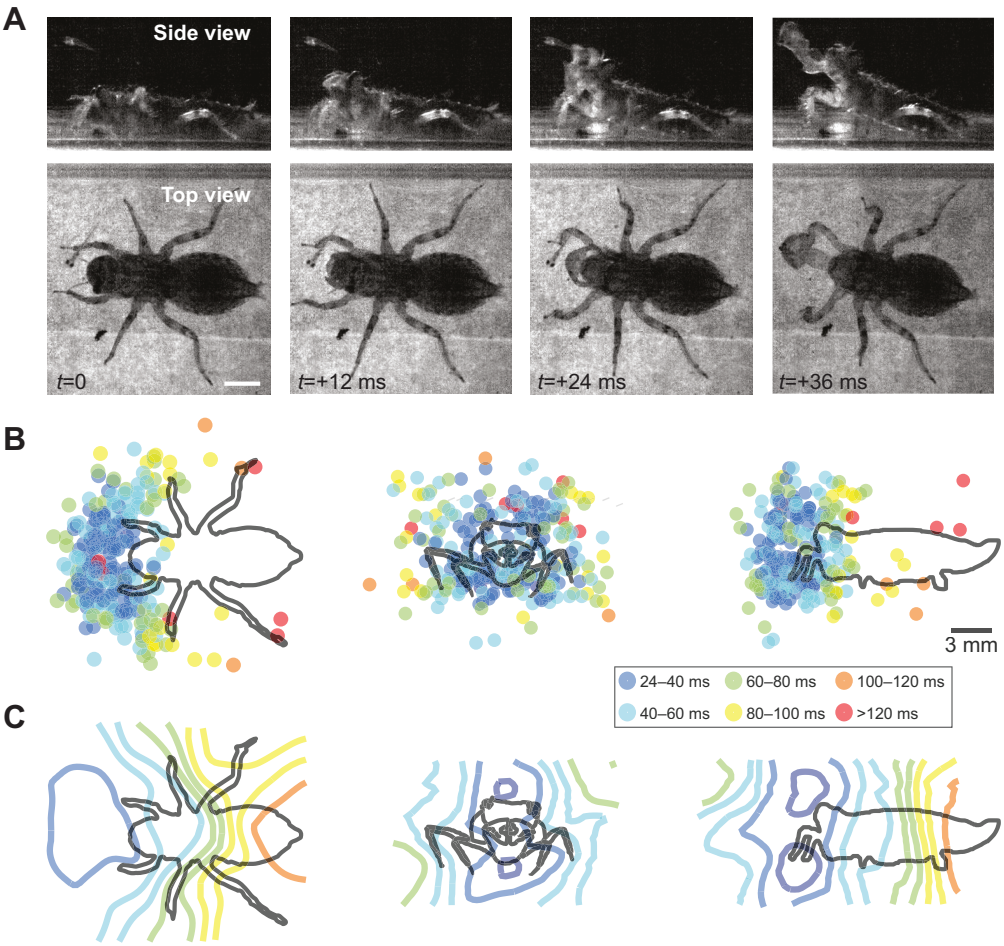

Fig. 1. Representative dragonfly nymph strike and prehensile mask motor volume. (A) Top and side view of a strike. Scale bar: 2.5 mm. (B) Top, front and side view orthographic projections of prehensile mask strike positions colored to represent the time duration of the strike. Scale bar: 3.0 mm. (C) Top (*x*–*y*), front (*y*–*z*) and side (*x*–*z*) view cross-sections of surfaces representing isochrones for the duration of the strike from the time of initial movement detected through high-speed videography. The three-dimensional isochronic surfaces define the prehensile mask motor volume.

(Liu and Fetcho, 1999; Burgess and Granato, 2007; Kohashi and Oda, 2008; Bhattacharyya et al., 2017).

Remarkably, upon analysis of various escape parameters, we found that the time remaining for the mask to intercept the fish once it initiated an escape was most predictive of the outcome. If the time to intercept is short, such as when a fish is too close to a nymph or a fish is further away but too delayed in its response to the nymph attack, death is more probable. We conclude that the interaction between the predator swept volume and the prey motor volume captures the influence of various escape maneuver parameters and provides a unique approach to analyze the utility of specific escape movements. We discuss how our results generalize to other predator–prey interactions and extend the existing understanding of the selective benefit of escape parameters along with their neural execution.

MATERIALS AND METHODS

Larval zebrafish

Experiments were performed using zebrafish [*Danio rerio* (F. Hamilton 1822)] larvae at 5–7 days post-fertilization (dpf) with body lengths of 4–5 mm, obtained from a laboratory stock of wild-type adults. At these early stages of development, zebrafish have not yet sexually differentiated. Fish in our custom-fabricated breeding facility (Aquatic Habitats, Beverly, MA, USA) were maintained at 28.5°C in system water (pH 7.3, conductivity 550 µS) on a 14 h:10 h light:dark cycle. All recordings of behavior were performed at room temperature (24°C) in system water. Animals were treated in accordance with the National Institutes of Health Guide for the Care and Use of Laboratory Animals and experiments were approved by the Northwestern University Institutional Animal Care and Use Committee.

Dragonfly nymphs

Dragonfly nymphs [*Sympetrum vicinum* (Hagen 1861)] were acquired from a commercial vendor (Carolina Biological Supply Company, Burlington, NC, USA). The age of the nymphs was unknown, but at this stage in development before metamorphosis, they have not yet sexually differentiated. Each nymph was stored at room temperature (24°C) in a separate tank with system water. Water in the tank was replaced weekly.

Behavior recordings

All recordings of behavior were performed at room temperature (24°C) in system water. Five dragonfly nymphs of approximately the same size were selected (body length mean±s.d.=14.5±1.3 mm) for all experiments since dramatic differences in size could change the size of the mask and the locomotor performance of the strike. For each experiment, a single dragonfly nymph was selected and placed into an arena within a square plastic dish (25 mm width, 100 mm length, 15 mm height, Thomas Scientific, Swedesboro, NJ, USA) with room temperature system water and allowed to acclimate for 15 min. The arena constrained the dragonfly nymph to move within the field of view of the dissection microscope (Stemi-2000; Carl Zeiss Microscopy, Thornwood, NY, USA). After acclimation, 1–5 larval zebrafish were introduced into the arena. More than one larval zebrafish was added to the arena in order to increase the chances of a strike from the nymph since it did not actively hunt the larva but chose

Journal of Experimental Biology (2021) 224, jeb235481. doi:10.1242/jeb.235481

to sit and wait until a larva came into striking distance. The dragonfly nymph would strike at a single zebrafish larva.

If the strike of the nymph was accurate and the larva initiated an escape response, the parameters of the fish escape responses were recorded. The strike of the dragonfly nymph was considered to be accurate if the labial mask extended to a final position ±2 mm from where the larval fish's swim bladder was immediately before the start of the strike. On the other hand, an inaccurate strike was one where the dragonfly nymph aimed its labial mask at a position where the fish was not present, even before the strike began. After a dragonfly nymph strike, the larvae were removed from the arena and new larvae were introduced in order to ensure that larvae were not acclimated to dragonfly nymph strikes.

To observe the dragonfly nymph strikes and fish escape responses in our assay, videos were recorded using a high-speed camera (FASTCAM 1024 PCI; Photron, San Diego, CA, USA) with a spatial resolution of 1024×1024 pixels attached to the microscope providing a top view into the arena. Additionally, a 100 mm long equilateral acrylic prism (Carolina Biological Supply Company, Burlington, NC, USA) was placed at the edge of the square Petri dish to provide a side view perspective into the dish within the same image. The top and side views used for imaging were calibrated with black lines 15 mm in length that were viewed from both top and side views. This allowed for a pixel to mm conversion. Both views had nearly the exact same mm pixel^{-1} (0.1 mm pixel^{-1}) conversion, suggesting that no extra corrections were necessary to account for the longer path length of the light in the side view perspective. The imaging set-up was not disturbed over the course of the experiments. Images were collected at 250 frames s^{-1} at 1× magnification.

For the top view, animals were illuminated from below with diffused white light from the microscope. Additional illumination was provided by a halogen lamp with an articulating arm from the side for the side view. The exact amount of illumination was not measured; however, we do not believe the visual systems of the dragonfly nymph or the zebrafish larvae were compromised since they both performed naturalistic behaviors.

Behavior analysis

A MATLAB (MathWorks, Natick, MA, USA) graphical user interface (GUI) was developed to manually track the orientation of the nymph and the position of the mask in top and side views. Tracking of the nymph was accomplished by selecting a point on the image at the center of the head between the eyes followed by the position of the anus immediately before the beginning of the strike. During the strike, the center of the nymph mask was also tracked over the course of its extension. The nymph's body and mask were tracked in top and side views. The orientation and total head yaw for the fish during the initial bend of the escape maneuver was also hand-tracked with a separate MATLAB GUI in side and top views. Larval fish were tracked by clicking on the head, the swim bladder and the end of the tail from the start of the escape response and through the initial bend. During the propulsive stage of the escape response, the fish was tracked with a MATLAB-based automated tracker to estimate swimming velocity for the subset of escape responses that remained within the field of view. The automated tracker used thresholding and blob-detection to track the fish over the course of the escape trajectory in the top and side views. Pixel positions in the two views were then transformed into their corresponding 3-dimensional (3D) coordinates. Since the top and side view were in the same image and shared a spatial axis, combining corresponding points in the top and side views into a single 3D point involved combining points along the shared axis. Our results are presented in nymph- or fish-centered coordinate systems depending on which coordinate system was more appropriate for analysis.

Dragonfly nymph prehensile mask motor volume model

The 3D position of each strike relative to the orientation of the dragonfly nymph body was computed with vector mathematics. Each point in the 3D point cloud of mask strike positions corresponded to a mask extension time: the time taken for the mask to reach that position in space (Fig. 1). A *k*-nearest neighbor (*k*-NN) model (Friedman et al., 1977) was used to estimate the mask extension time given a 3D position.

The *k*-NN model estimates the value of the mask extension time given a point in 3D space using the known mask extension time of the *k* nearest neighbors to the point of interest. We tested integer values of *k* ranging from 1 to 10. We performed 10-fold cross validation for these integer values of *k* by splitting the dataset into 10 parts and using 9 of the parts to predict the time needed to reach the 3D positions in the last part. This cross validation was done for each part, for each value of *k*, to see which value of *k* provided the predictions with the lowest mean-squared error. We found the lowest overall error with k=5 and used this value to generate the prehensile mask motor volume seen in Fig. 1C.

Neomycin treatment of larval zebrafish

We tested the role of flow sensing in fish escape responses by compromising the lateral line in a group of larvae by exposure to a 250 µmol l^{-1} solution of neomycin sulphate (Sigma Aldrich, St Louis, MO, USA) for a 30 min period, followed by a 3 h recovery prior to experiments. This technique was developed in previous studies (Harris et al., 2003; McHenry et al., 2009), where it was shown to induce cell death in lateral line hair cells while leaving inner ear hair cells intact. However, we allowed for a longer recovery period after neomycin treatment to ensure recovery. After recovery, larval fish were monitored to confirm that they performed spontaneous swimming behaviors and responded with escape maneuvers to touch stimuli delivered with a tungsten filament. These larvae were then introduced into the dish with the dragonfly nymph and tested as described above.

Approximating fluid velocity at the fish due to mask extension

To gain further insight into the role of the perturbed fluid due to mask extension in generating the fish escape response, we used a potential flow approximation to estimate the fluid velocity at the fish position due to mask extension. Mask velocity alone was not a good proxy for the perturbed fluid flow at the fish position since it does not take into account the distance of the fish from the mask. We started with an established analytical solution to the flow velocity field expressed in spherical coordinates around a sphere of radius a moving through an incompressible, inviscid fluid at a time dependent velocity $V(t)$ (Fitzpatrick, 2017):

$$v_r(r,\theta,t) = V(t)\frac{a^3}{r^3}\cos\theta \ , \quad (1)$$

$$v_\theta(r,\theta,t) = \frac{1}{2}V(t)\frac{a^3}{r^3}\sin\theta \ , \quad (2)$$

$$v^2 = v_r^2 + v_\theta^2 \ , \quad (3)$$

where v is the flow velocity expressed in terms of the radial and angular components, v_r and v_θ, for a position at some distance $r \geq a$

and angle θ from the sphere with respect to its velocity vector at some time t. We expect the flow pattern around the sphere to be axisymmetric around the velocity vector (i.e. independent of ϕ). In this set of equations, we can verify that when $r \to \infty$ then $v \to 0$, as we would expect. We used these equations with the velocity of the tracked labial mask as the value for $V(t)$ to estimate the flow velocity v at the fish which was some distance $r \geq a$ and angle θ. The value of a was set to 1.6 mm which approximated the radius of the smallest circle enclosing the frontal projection of the mask (average diameter of 3.2 mm across all specimens).

In certain cases, the dragonfly nymph would also have to move its head during the mask extension which is not accounted for here. However, the head movement of the nymph is expected to contribute minimally to the already intense hydrodynamic stimulus from the extending mask.

We used this potential flow approximation since our intention was not to compute the exact magnitudes of flow velocities. Rather, we investigated how relatively higher and lower flow velocities influenced the fish escape response.

Predicting escape outcome with each parameter

We parameterized the dragonfly nymph strike and the fish escape response to determine which parameter had the most influence on the fish escape outcome. The specific statistical tests used to determine the influence of parameters are described in the Results. To investigate the interaction of escape maneuver parameters, we trained random forest classifiers (Breiman, 2001). Random forest classifiers build an ensemble of decision trees to predict a target variable (escape success or failure) based on the values of predictors (attack azimuth, attack elevation, mask extension time, etc.). They do this by bootstrapping the dataset (sub-selecting from features and data points) to build a decision tree for each bootstrapped sample. Each decision tree generates a prediction for the target variable, and votes from the ensemble are aggregated for the final prediction. Classifiers were built with each of the following parameters to predict the binary outcome of escape failure (0) or escape success (1): (i) attack azimuth: the azimuth (−180 deg to 180 deg) of the dragonfly nymph strike relative to the orientation of the larval zebrafish; (ii) attack elevation: the elevation (−180 deg to 180 deg) of the dragonfly nymph strike relative to the orientation of the fish; (iii) mask extension time: the time needed to extend the mask to where the fish was located just before the initiation of an escape response; (iv) bend duration: the duration of the initial bend of the larval zebrafish escape response; (v) bend velocity: the velocity in deg ms^{-1} of the initial bend of the larval zebrafish escape response; (vi) response latency: the latency of the fish escape response from the start of the nymph's strike; and (vii) time to intercept after threat response: the time left from the initiation of the fish escape response until the mask reaches the initial position of the fish.

Ten different classifiers were trained for each parameter by pseudo-randomly selecting 85% of the dataset each time for training the classifier, and the remaining 15% of the dataset was used for testing the accuracy of the trained classifier. This procedure estimated the mean±s.e.m. of accuracy for a classifier built on a single parameter.

To understand the interaction of parameters, 10 classifiers were also trained using all of the parameters as predictors with the same process of splitting the data as described. The parameter importance was computed by the random forest classifier algorithm (Breiman, 2001). Intuitively, parameter importance is estimated by randomly permuting the values of each of the features to see how dramatically it changes the model predictions. The most important feature will have the most negative impact on the predictions when randomly permuted. Therefore, the features are ranked by how their random permutations impacts the predictions.

Random forest classifiers were chosen over other classifiers due to their simplicity, their ability to perform non-linear classification, and exploit interactions between features while reducing variance through bootstrapping. Moreover, random forest classifiers are able to provide importance values for each predictor which was especially useful.

Computational motor volume of larval zebrafish

We computationally simulated the larval zebrafish motor volume to investigate how the intersection of the motor volume of larval zebrafish with the swept volume of the dragonfly nymph mask influenced the likelihood of survival for the fish. We used the non-engulfed fraction of the larval zebrafish motor volume as a measure of the survival likelihood of the fish.

During an escape response, larval zebrafish reorient with an initial bend with little or no movement of their center of mass and swim away with undulatory, propulsive swimming (Nair et al., 2015). In this study, the fish motor volume was computationally generated to mimic this movement using a bend velocity (in deg ms^{-1}) and a propulsive velocity (in mm ms^{-1}). The bend velocity was first used for reorientation and then the propulsive velocity was used to compute the distance traveled. In this manner, the rotation from the bend velocity and translation due to the propulsive velocity together could define the positions in 3D space that the center of mass of the larval zebrafish could reach given a certain amount of time. For all simulations of fish motor volumes, the propulsive velocity used was 0.12 mm ms^{-1}, which is supported by existing literature (Budick and O'Malley, 2000; Dunn et al., 2016). We assumed that the fish could reorient in any direction by changing pitch and yaw as necessary, which was supported by our own data and existing literature (Nair et al., 2015).

We did not account for bend acceleration and propulsive acceleration. These accelerations would largely influence the estimates of rotation and translation at the initiation of the escape response but leave other estimates unchanged. Moreover, these accelerations are not well reported for larval zebrafish.

Representative fish motor volumes for visualization were generated using the average bend velocity of 14 deg ms^{-1} as found in this study. The average bend velocity was used to base the representative fish motor volumes on the measured kinematics.

To understand how the intersection of the fish motor volume with the swept volumes of the nymph mask influenced the likelihood of survival, we needed to create fish motor volumes that adequately represented the diversity of fish kinematics measured. To this end, we pseudo-randomly sampled with replacement the initial bend velocities measured in this study for six increments of time to intercept (7, 15, 20, 25, 35 and 50 ms) within the observed range. Fifty of these fish motor volumes were generated for each increment of time to intercept and then used to compute the proportion of the fish motor volume not engulfed by the mask.

The swept volume of the mask was represented by a hemi-ellipsoid (major axis: 3.2 mm and minor axis: 2.8 mm) attached to the end of a half-cylinder (diameter: 3.2 mm and length: 6 mm) whose dimensions were determined by measuring the prehensile masks of specimens in this study. To intersect the mask swept volume with the fish motor volume, the center of the hemi-ellipsoid of the mask swept volume was placed at the starting position of the fish motor volume. We simulated attacks from different directions with combinations of attack azimuths (front, side and behind) and elevations (in-plane, above and below) by rotating the mask swept

volume around the origin of the fish motor volume. Ten thousand points were pseudo-randomly generated within the fish motor volume and the proportion of points not within the mask swept volume provided a measure of the proportion of the fish motor volume not engulfed. This was carried out for each fish motor volume for each increment of time to intercept to find the mean±s.d. proportion not engulfed. Fish motor volumes representing Mauthner active and silent responses were generated by pseudo-randomly sampling different uniform distributions of initial bend velocities. The range of bend velocities for Mauthner silent motor volumes was 10±5 deg ms^{-1} and for Mauthner active motor volumes it was 18±5 deg ms^{-1} based on prior studies that investigated bend velocities of free swimming larval zebrafish before and after Mauthner ablation (Liu and Fetcho, 1999; Burgess and Granato, 2007; Hecker et al., 2020). The ranges were also constructed to have some overlap since studies have found that Mauthner active and silent responses can on occasion produce similar kinematics (Kohashi and Oda, 2008; Bhattacharyya et al., 2017). The simulated propulsive velocity was not changed for Mauthner active motor volumes since the effect of Mauthner cell activation on propulsion is not clear (Nissanov et al., 1990; Eaton and Emberley, 1991; Neki et al., 2014; Dunn et al., 2016).

Intersections of the Mauthner active and silent motor volumes with the prehensile mask swept volume were carried out in the way described above. The MATLAB code used to generate and visualize larval zebrafish motor volumes and the mask swept volume have been published separately (Bhattacharyya et al., 2020).

Statistical methods

The statistical tests used to test hypotheses and their associated *P*-values are reported within the Results with references to each figure panel. The *P*-values are also repeated within the Results section when discussing those hypotheses and the results of the statistical test. We considered $P<0.05$ to be significant. Within the figure panels, asterisks are used to represent *P*-values in the corresponding manner: *$P<0.05$, **$P<0.01$ and ***$P<0.001$.

We have used Mann–Whitney *U*-tests when comparing two populations to test whether one population tends to have values larger than the other. When comparing the variances of two populations, we have used Levene's test. In scenarios where we compared a population of measurements against a specific value, we have used the one-sample Wilcoxon signed rank test which is a non-parametric alternative to the one-sample *t*-test. Whenever these tests were repeated in a pair-wise manner, we performed a Bonferroni correction to the threshold *P*-value of 0.05 by dividing by the total number of unique pairs. When comparing the medians of more than two populations, we have used the Kruskal–Wallis *H* test. Finally, in one instance, we have compared the changing probability of a successful escape as a function of the time to intercept with the changing fraction of the fish motor volume not engulfed as a function of time to intercept with an analysis of covariance test. This test compares the slope and intercept of two regression lines, allowing for a measure of whether escape success probability and the non-engulfed fish motor volume are significantly different functions of the time to intercept.

RESULTS

Dragonfly nymph prehensile mask motor volume and attack outcome

To evaluate predator–prey interactions, we filmed strikes of nymphs upon larval zebrafish at 250 frames s^{-1} with top and side view perspectives (Fig. 1A). To quantify the biomechanical performance of the attack, we studied the duration of the predatory strike with respect to the furthest point reached by the prehensile mask in 3-dimensional (3D) space. The mask extension times ranged from 24 to 176 ms depending upon the location of the strike (number of strikes=159). The time needed for the mask to reach specific positions in space (Fig. 1B) was well described by a *k*-NN model (R^2=0.7, Fig. 1C, see also Materials and Methods), which served as a representation of the motor volume of the mask: the volume swept by the appendage over all strikes within a given amount of time (Snyder et al., 2007). As seen in the cross-sections of the isochronic surfaces of the motor volume (Fig. 1C), strikes directed towards lateral and caudal positions took more time than strikes directed medially and rostrally. This model represents the maneuverability of the mask, providing insight about the time-scale and directional bias of predatory strikes.

To see how the outcome of the attack was influenced by aspects of the predatory encounter, we categorized the interactions. Successful and failed captures had distinct spatial distributions of the position of the fish before the attack (Fig. 2A), where nymphs were more likely to capture larvae in closer proximity. We found different kinds of failed and successful captures (Fig. 2B). A failed capture could occur either because of an error in the predatory attack or an effective escape executed by the fish. A successful capture occurred either owing to a fish not responding or an ineffective escape attempt (Fig. 2B).

The nymph strike was inaccurate in some instances when the fish performed spontaneous swimming movements just before the start of a predatory strike (more commonly, the fish was stationary immediately preceding the initiation of the strike). In these cases, the dragonfly nymph would strike at positions where the fish was no longer present (Fig. 2B, tactile delay, visual delay). A tactile delay refers to an inaccurate strike aimed at a part of the dragonfly nymph body that was touched by a spontaneously swimming fish some time before the strike began. A visual delay refers to an inaccurate strike aimed at a position previously occupied by a spontaneously swimming fish before the attack started.

Each case allowed for a measurement of the sensorimotor delays of the nymph. For tactile stimuli, this delay was 75.5±30 ms (n=16 strikes), and for visual stimuli, it was 278±110 ms (n=5 strikes). This suggests that the nymph is not ballistically intercepting the prey by predicting its future location, but rather striking at the position of the prey before the attack began. Sometimes, the nymph also made targeting errors where the fish was stationary through the entire strike, but the strike was aimed inaccurately (Fig. 2B, targeting error, see Fig. S1).

While attack errors provide information about the sensorimotor limitations of the dragonfly nymph, they cannot help to determine the relevant escape decisions of the fish that confer success. Thus, we focused the remainder of our analysis on the instances where the mask was correctly aimed at the position of the fish prior to the initiation of the attack.

Likelihood of a response from zebrafish larvae to accurate strikes

To investigate the sensorimotor performance of the fish, we studied the likelihood of a fish initiating an escape response given an accurate strike. The spatial distributions of the fish positions before the start of the predatory strike were different for scenarios where the fish responded or did not respond (Fig. 3A). Fish with initial positions closer to the nymph mouth were less likely to produce a response (Fig. 3A).

For Fig. 3B–E, we estimated the fish response probability by averaging the fraction of escape-producing strikes from each nymph. We tested 5 nymphs and each nymph made 15–30 strikes

Journal of Experimental Biology (2021) 224, jeb235481. doi:10.1242/jeb.235481

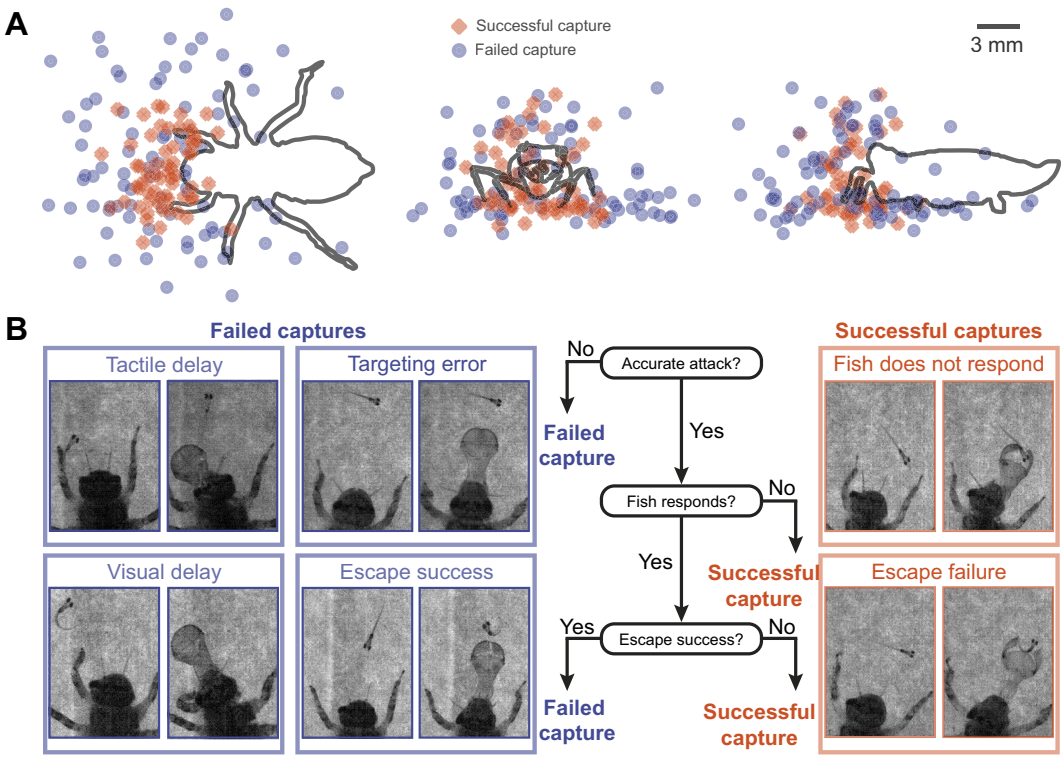

Fig. 2. Causes of successful or failed captures by the nymph. (A) Top (*x*–*y*), front (*y*–*z*) and side (*x*–*z*) view orthographic projections of 3D initial fish positions before the start of the nymph's strike with points colored to represent the outcome of a successful or failed capture by the nymph. (B) Process diagram demonstrating the sequence of events and causes of a successful or failed capture by the nymph with representative examples of each branching event in the process.

aimed correctly at the fish. The azimuthal or elevation position of the nymph mouth with respect to the fish had little or no influence over the response probability of the fish (Fig. 3B, Kruskal–Wallis *H* test P=0.95; and Fig. 3C, Kruskal–Wallis *H* test P=0.85, number of nymphs=5 for all groups). However, the fish was more likely to respond given longer mask extension times (Fig. 3D, Kruskal–Wallis *H* test, P=0.02, number of nymphs=5 for each group with error bars). The reduced likelihood of responding to short extension times may be because fish were captured before the initiation of a response could begin. Regardless, since the response probability was consistently above 50%, fish were always more likely to respond than not respond.

To understand whether the larval fish were initiating escape responses only on the basis of flow stimuli or a combination of visual and flow stimuli, we tested the role of flow sensing by compromising the lateral line in a group of larvae with exposure to neomycin sulphate (see Materials and Methods). All neomycin-treated fish failed to respond to any strikes (Fig. 3E, Mann–Whitney *U*-test, P=0.003, number of nymphs=5 for treated and 4 for untreated group). These data suggest that fish generate escapes in this scenario largely on the basis of flow sensing and do so with high likelihood regardless of relative orientation and position with respect to the nymph.

To better understand how the perturbed fluid movement due to the strike influenced the larval zebrafish response (Fig. 4A), we tracked the 3D position of the mask for all strikes that produced an escape response in fish. The perturbed fluid velocity in water around a moving body, such as a sphere, is a function of the velocity of the body and the distance from the body (Fig. 4B, see Materials and Methods). To account for both velocity and distance when estimating the fluid flow experienced by fish, we used the mask velocity (Fig. 4C) to estimate the perturbed fluid velocity over time at the initial fish position (Fig. 4D). Since the distance to the initial fish position from the mask reduced as the mask extended, the perturbed fluid velocity at the initial fish position approached the velocity of the mask (Fig. 4D). Different mask extension times had different velocity and associated fluid velocity profiles (Fig. 4E–G, Strike ≤28 ms n=27, 28 ms <Strike ≤44 ms n=24, Strike >44 ms n=15). The mean response latency of the fish and the variance of response latency both increased with increasing mask extension times (Fig. 4E–G, Kruskal–Wallis *H* test, P=0.01, pair-wise Levene's test with Bonferroni correction, all $P \leq 0.01$). We further investigated how larval zebrafish escape responses were effected by the earliest fluid perturbations caused by the prehensile mask. Fish responded with shorter and less variable response latencies to the fastest quartile of fluid velocities computed between 0 and 4 ms after the onset of the attack (Fig. 4H, Mann–Whitney *U*-test P=0.002, Levene's test, P=0.0003, n=18 for both groups), hereafter referred to as the initial fluid velocity.

During the escape response, the fish changed heading direction with an initial bend and then swam away with propulsive swimming. To test whether the initial fluid velocities experienced by the fish influenced the kinematics of the escape response, we measured the bend angle (Fig. 4I) for all responses where the fish clearly finished the initial bend. The bend angle was not significantly different between the fastest and slowest quartile of initial fluid velocities (Fig. 4J, Mann–Whitney *U*-test and Levene's test, all P>0.3, n=15 for both groups). However, the fastest initial fluid velocities did produce responses with significantly faster bend velocities (Fig. 4K, Mann–Whitney *U*-test, P=0.02, n=15 for both groups). All initial bend durations recorded fell between 4–8 ms (n=33), 8–12 ms (n=22) or 12–16 ms (n=2) after the onset of the escape. Escapes with shorter bend durations (≤8 ms) tended to be in response to significantly

Journal of Experimental Biology (2021) 224, jeb235481. doi:10.1242/jeb.235481

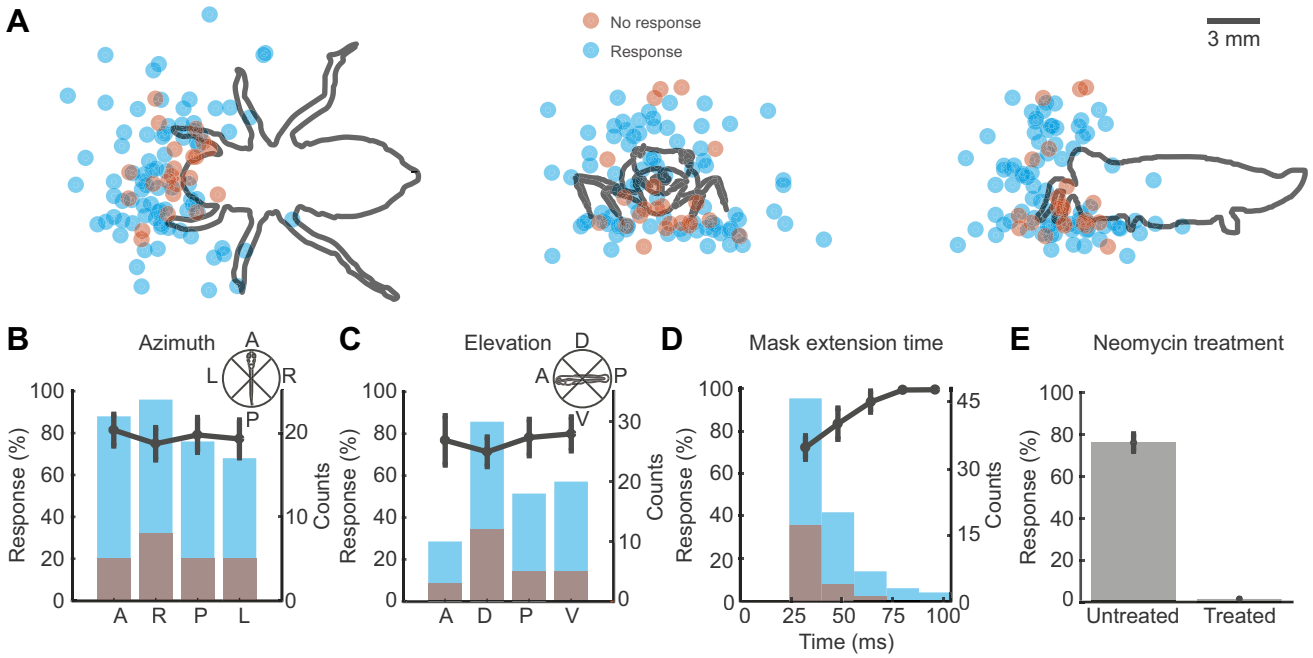

Fig. 3. Likelihood of larval zebrafish response to an accurate strike. (A) Top (*x*–*y*), front (*y*–*z*) and side (*x*–*z*) view orthographic projections of 3D initial fish positions before the start of an accurate strike with points colored to represent whether the fish responded. (B–D) Height of overlapping bars represents the count of strikes within that bin (right *y*-axis) and the color represents whether the fish responded or not. The line plot shows the mean±s.e.m. fish response probability averaged by nymph for each bin (left *y*-axis). (B) Fish response probability based on the azimuthal position of the nymph head with respect to the fish. There are no significant differences between response probabilities for each azimuthal quadrant. (C) Fish response probability based on the elevation of the nymph head with respect to the fish. There are no significant differences between response probabilities for each elevation quadrant. (D) Fish response probability based on the mask extension time to the fish position. The fish is significantly more likely to respond for longer extension times. (E) Overall response probability of neomycin-treated fish and untreated fish. Neomycin-treated fish are far less likely to respond to a strike than untreated fish. All data are means±s.e.m. A, anterior; D, dorsal; L, left; P, posterior; R, right; V, ventral.

higher initial fluid velocities (Fig. 4L, Mann–Whitney *U*-test, P=0.008, ≤8 ms n=33, >8 ms n=24). These data suggest that fish modulate their escape responses with different latencies and kinematics based on the magnitude of perturbation.

Larval zebrafish position, orientation and escape direction

We next examined how the position and orientation of the fish at the start of the attack, along with its escape direction, influenced escape success. The spatial distribution of the fish positions before the start of the predatory strike for successful and failed escapes largely overlapped but failed escapes tended to happen closer to the nymph (Fig. 5A). For Fig. 5B–D, we estimated the escape success probability by averaging the fraction of nymph strikes from which fish generated and executed successful escapes. We tested 5 nymphs and each nymph made 14–25 strikes aimed correctly at the fish where the fish generated an escape response (excluding scenarios where the fish did not respond).

The azimuthal quadrant of the attack with respect to the fish had no significant influence on escape success probability (Fig. 5B, Kruskal–Wallis H test, P=0.4, number of nymphs=5 for all groups). However, the attack elevation was significantly related to the escape success probability (Kruskal–Wallis H test, P=0.01, number of nymphs=5 for all groups). Specifically, fish were significantly more likely to execute successful escapes when responding to attacks from below (ventral, V) than from above (dorsal, D; Fig. 5C, Mann–Whitney *U*-test, P=0.005, number of nymph=5 for both groups). Moreover, fish were more likely to execute successful escapes in response to longer mask extension times (Fig. 5D, Kruskal–Wallis H test, P<0.001), which is consistent with the higher probability of escaping at further distances or with more time.

We then analyzed the influence that the directionality of attacks and escapes had on escape success. Escape directions in the opposite hemisphere of the attack quadrant were considered to be away from the attack. For Fig. 5F and I, we estimated the probability of escaping away from the attack by averaging the fraction of strikes from each nymph where the fish escaped away.

When escape directions were grouped by the azimuthal or elevation attack quadrants (Fig. 5E,H), fish did not consistently move away from the attacks. Escapes in response to attacks from the right (R), posterior (P), and left (L) azimuthal quadrants were not significantly biased away from the attack (Fig. 5F, one-sample Wilcoxon signed rank test with Bonferroni correction, P>0.3, number of nymphs=5 for all groups). Similarly, escape directions in response to attacks from the dorsal (D) and posterior (P) elevation quadrants were not significantly biased away from the attack (Fig. 5I, one-sample Wilcoxon signed rank test with Bonferroni correction, P>0.3). While fish did significantly bias their escape directions away from attacks in the anterior (A) azimuthal and elevation quadrants (P<0.001), this could be because escape movements typically involve a turn (Bhattacharyya et al., 2017), especially those in response to attacks directed at the head (O'Malley et al., 1996). The lack of consistent directional control was also illustrated by the fact that larvae would often escape in the direction of attacks occurring in the ventral (V) elevation quadrant (Fig. 5I). Critically, whether fish escaped away or towards the attack had no significant influence on escape success probability (Fig. 5G,J, Mann–Whitney *U*-tests, all P>0.5, number of nymphs=5 for all groups). However, escape trajectories toward the attack can occur along pitch or yaw angles that take the fish around the mask, thereby keeping the fish out of the capture zone.

Journal of Experimental Biology (2021) 224, jeb235481. doi:10.1242/jeb.235481

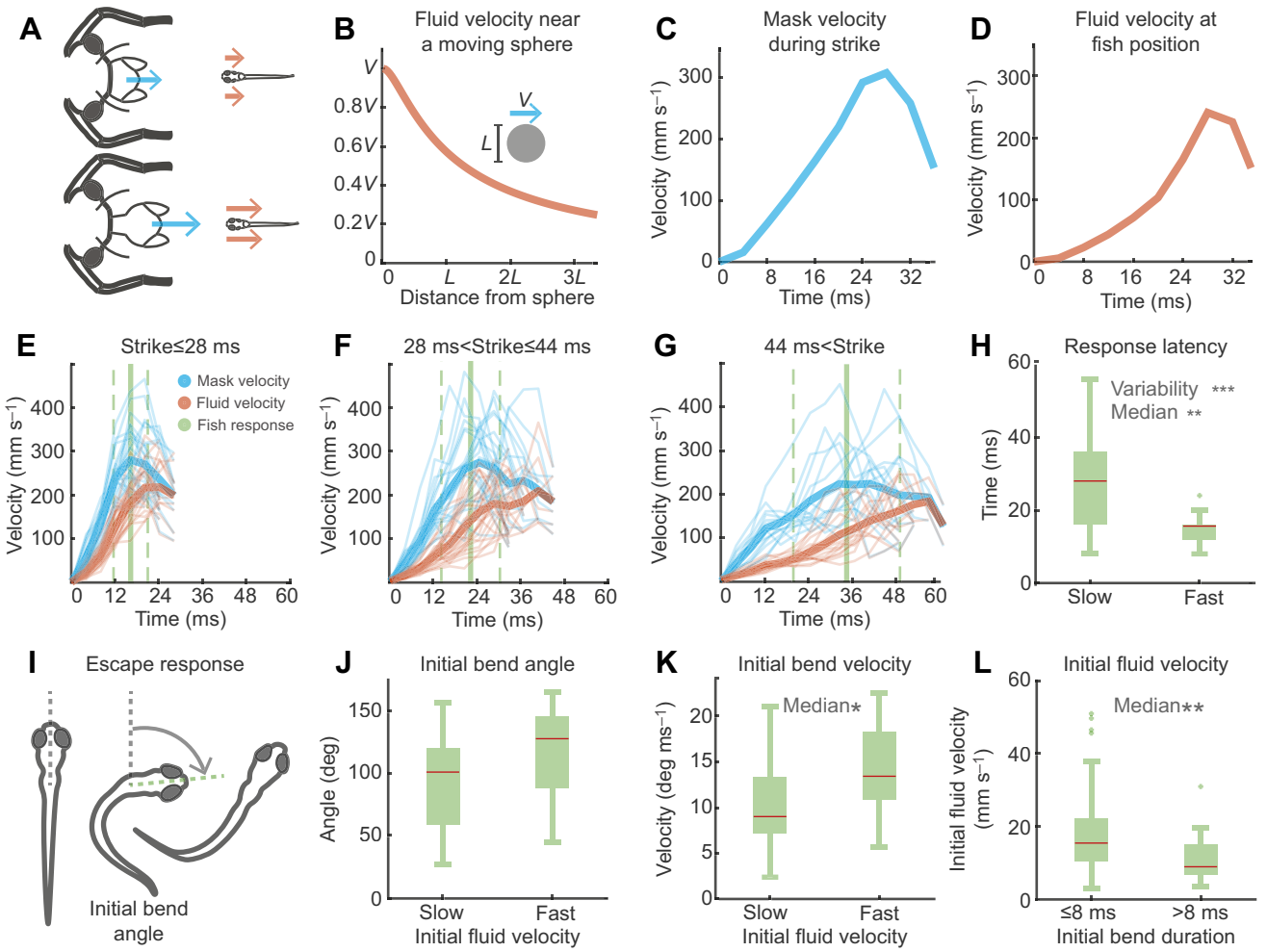

Fig. 4. Larval zebrafish responding to fluid movement from the nymph's strike. (A) The mask velocity (in cyan) and the estimated perturbed fluid velocity at the fish position (in orange) both change over the duration of the strike. (B) The perturbed fluid velocity at some distance from the edge of a sphere with diameter *L* moving at velocity *V* was estimated (see Materials and Methods). The fluid velocity at the fish position depends on both the mask velocity and the distance from the mask. (C) A representative example of mask velocity during an accurate strike. (D) The corresponding estimated fluid velocity at the initial fish position computed from the measured mask velocity and the potential flow approximation. (E–G) Mask (cyan) and fluid velocity (orange) profiles of different strikes grouped by the mask extension time with the mean±s.d. of larval zebrafish response times (green solid and dashed vertical lines). Lighter lines represent individual velocity profiles while bold lines represent the mean for each group. (H) Larval zebrafish response latencies grouped by slow (first quartile) and fast (fourth quartile) fluid velocities at the fish position 0–4 ms after onset of the attack. (I) During the escape response, the fish changes heading direction with an initial bend and then swims away with propulsive swimming. The initial bend angle is the angle between the heading vector of the fish before the start of the escape response and the heading vector at the end of the initial bend. Responses where it was unclear whether the fish completed the initial bend before being captured were excluded from analysis of initial bend parameters. (J) Initial bend angles of responses grouped by slow (first quartile) and fast (fourth quartile) fluid velocities at the fish position after onset of the attack. There is no significant difference between the two groups. (K) The initial bend velocity of responses grouped by slow (first quartile) and fast (fourth quartile) fluid velocities at the fish position after onset of the attack. Initial bend velocities of responses to fast fluid velocities are significantly higher than those to slow fluid velocities. (L) Fluid velocity at the fish position after onset of the attack grouped by initial bend durations ≤8 ms and >8 ms. Initial bend durations ≤8 ms occur in response to significantly higher initial fluid velocities at the fish. Data in H and J–L are box-and-whisker plots, where the red line is the median, and the box extends from the 25th to 75th percentiles; whiskers extend to the most extreme data points not considered outliers; **P*<0.05, ***P*<0.01 and ****P*<0.001.

Together, these data suggest that the escape direction relative to the attack direction was not significantly related to escape success probability, and in some cases, escapes toward attacks were successful. Thus it seems more important that zebrafish move quickly rather than in the opposite direction.

Importance of time to intercept after threat response

Having found that the escape direction of the larval fish had no discernible influence on escape success, we next explored how the fish's response latency may have influenced the escape outcome. Surprisingly, the response latencies of successful and failed attacks were not significantly different (Fig. 6A, Mann–Whitney *U*-test, Levene's test, all $P>0.8$, Escape fail $n=43$, Escape success $n=37$). To investigate how this discrepancy might be explained, we examined in more detail how response latency may interact with mask extension time. We defined the time left from the initiation of the fish escape response until the mask reaches the initial position of the fish as the time to intercept after threat response (Fig. 6B). The time to intercept was dramatically different for successful and failed escapes (Fig. 6C, Mann–Whitney *U*-test, $P\ll0.0001$; escape fail $n=43$, escape success $n=37$). Additionally, the escape success probability increased with increasing time to intercept (Fig. 6D, Kruskal–Wallis *H* test $P\ll0.001$, $n=21$ for all points).

Journal of Experimental Biology (2021) 224, jeb235481. doi:10.1242/jeb.235481

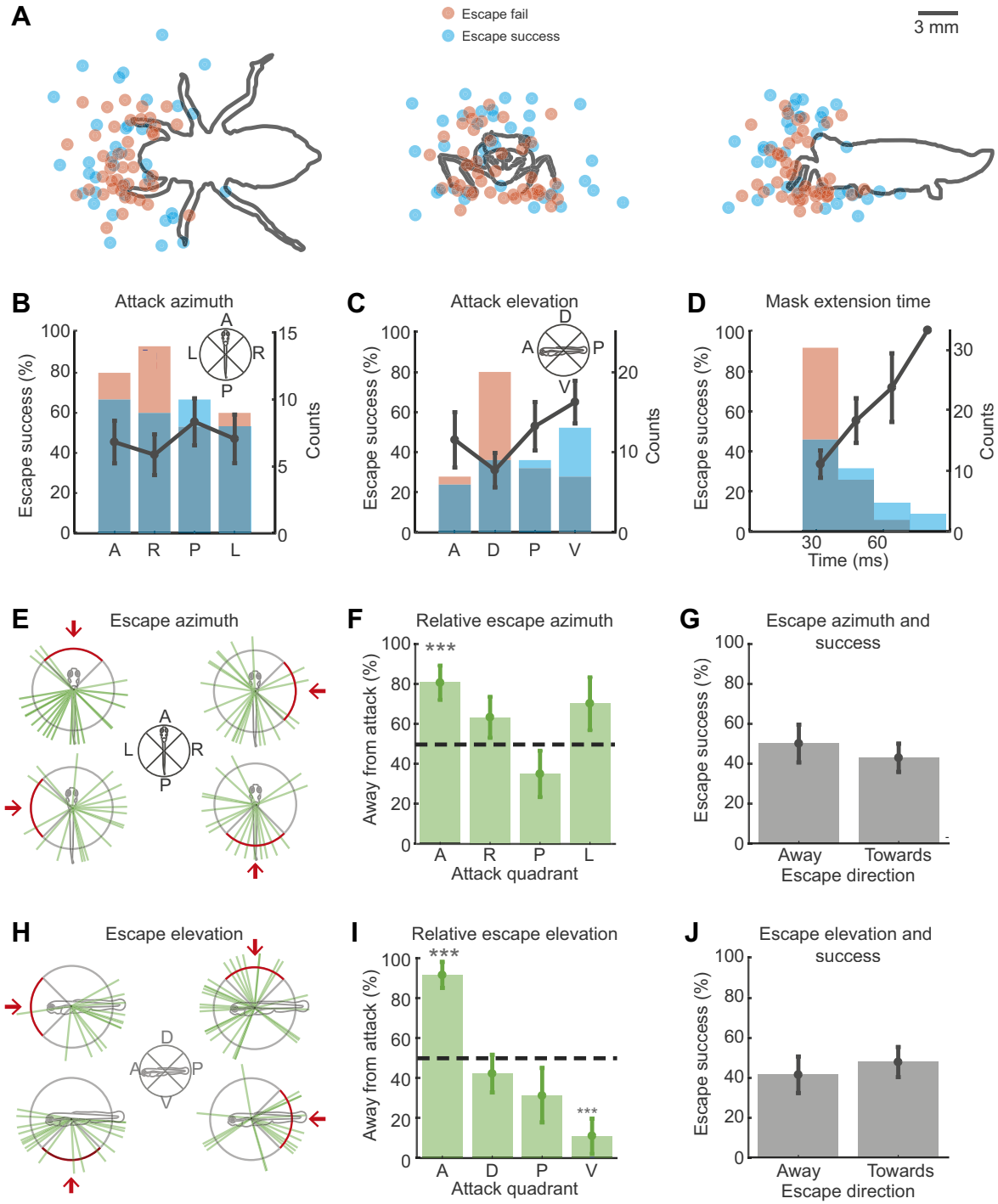

Fig. 5. See next page for legend.

To further investigate the interaction of escape maneuver parameters and which single parameter, if any, had the most influence on the outcome, we trained different random forest classifiers with each parameter to predict escape success or failure (see Materials and Methods). A naive estimate which predicted that all escapes failed had an accuracy of 0.55 (gray dashed line, Fig. 6E). Any classifier trained on one of these parameters with a significantly higher classification accuracy suggested that the parameter had some influence on the outcome. The classifiers trained on attack elevation, mask extension time, bend velocity, and time to intercept had classification accuracies significantly different from the naive estimate. However, the classifier trained on time to intercept after threat response dramatically outperformed all other classifiers (pairwise Mann–Whitney *U*-tests with Bonferroni correction, all $P<0.005$, $n=10$ for all groups) and was not significantly different from a classifier trained on all of the parameters together (pink dashed line, Fig. 6E, Mann–Whitney *U*-test, $P=0.4$, $n=10$ for both groups). As a further test, a random forest classifier trained on all of the parameters together was used to determine which parameter was the most important in determining

Journal of Experimental Biology

Fig. 5. Larval zebrafish position, orientation and escape direction. Top (*x*–*y*), front (*y*–*z*) and side (*x*–*z*) view orthographic projections of 3D initial fish positions before the start of an accurate strike with points colored to represent whether the fish escape response failed or succeeded in evading capture. (B–D) Heights of bars represent the count of strikes within that bin (right *y*-axis) and the color represents whether the fish escape failed or succeeded. The line plot shows the mean±s.e.m. fish escape success probability for each bin (left *y*-axis). (B) Fish escape success probability based on the azimuthal quadrant of the strike with respect to the fish. There are no significant differences in escape success probability with respect to attack azimuth. (C) Fish escape success probability based on the elevation quadrant of the strike with respect to the fish. Fish escapes are significantly more likely to succeed when responding to attacks from quadrant V (ventral) than from quadrant D (dorsal). (D) Histogram demonstrating the fish escape success probability based on the mask extension time to the fish position. Fish escapes are more likely to succeed as mask extension times increase. (E) The azimuthal direction of fish escape represented by green lines and grouped by the azimuthal quadrant of the strike. (F) Escape azimuth of fish relative to the azimuthal quadrant of the attack. The height of the bars represent the mean±s.e.m. probability of fish escaping away to the opposite azimuthal hemisphere from the attack quadrant. Asterisks represent significant difference from 50% (dashed line). (G) The azimuthal direction of fish escapes grouped by whether the response was directed towards the opposite azimuthal hemisphere or towards the same azimuthal hemisphere containing the azimuthal quadrant of attack. There is no significant difference in escape success between responses with azimuthal directions towards or away from the strike azimuth. (H) The elevation direction of fish escape represented by green lines and grouped by the elevation quadrant of the strike. (I) Escape elevation of fish relative to the elevation quadrant of the attack. Asterisks represent significant difference from 50% (dashed line). (J) The elevation of fish escapes grouped by whether the response was directed away from or towards the elevation direction of the strike. There is no significant difference in escape success between responses with elevation directions towards or away from the strike. Data in F,G,I,J are means±s.e.m.; ***P<0.001

the model prediction (see Materials and Methods). The importance of time to intercept after threat response as a parameter was dramatically higher than all other parameters in determining the model prediction (Fig. 6E).

These data suggest that even though various parameters were correlated with escape outcome, the time to intercept was the best and most important predictor of the escape outcome (Fig. 6E,F).

Fish motor volume at the time to intercept

The time to intercept after threat response limits the volume of space that contains all possible trajectories of the fish. This constraint is visible in the cross-sections of isochronic surfaces (computationally generated, see Materials and Methods), representing the fish motor volume for different times to intercept (Fig. 7A). These isochrones quantify the maneuverability of the fish (Snyder et al., 2007) within that time. Using this model, we visualized the portions of the fish motor volume not engulfed by the swept volume of the mask (Fig. 7B). The non-engulfed fraction of the fish motor volume represents the regions of space visited during a successful escape. We hypothesized that the importance of the time to intercept in determining the outcome was due to its direct influence on the fish motor volume and its intersection with the mask swept volume.

We used simulations to investigate how the fraction of the fish motor volume not engulfed by the mask volume corresponded to the escape success probability (Fig. 6D). Fifty virtual fish motor volumes were intersected with virtual mask swept volumes attacking from different directions (see Materials and Methods). The increase in the proportion of the fish motor volume not engulfed with increasing time to intercept corresponded well to the increase in the measured escape success probability (Fig. 7C). Moreover, an analysis of covariance demonstrated that the fraction of the motor volume not engulfed and the proportion of successful escape responses as a function of the time to intercept were not significantly different (slope, P=0.4; intercept, P=0.2).

We used the proportion of the fish motor volume not engulfed to computationally investigate the utility of recruiting the Mauthner cell in generating a response. We generated virtual Mauthner-active and Mauthner-silent fish motor volumes using different ranges of initial bend velocities (see Materials and Methods). The Mauthner-active motor volumes were consistently larger than the Mauthner-silent motor volumes for all times to intercept (Fig. 7D). The greatest difference between the Mauthner-active and Mauthner-silent motor volumes were seen for the shortest times to intercept (Fig. 7E). This is because the parameters for the Mauthner-active motor volume allowed the virtual fish to finish the initial bend earlier and start propulsion, which rapidly increases the motor volume.

Mauthner-active and Mauthner-silent motor volumes were also intersected with the swept volume of the nymph mask to compute the proportion of the fish motor volume not engulfed (Fig. 7F, refer to Materials and Methods). The proportion of the Mauthner-active fish motor volume not engulfed was significantly different from the proportion of the Mauthner-silent motor volume not engulfed (two-way ANOVA; Mauthner recruitment P<0.001; time to intercept, P<0.001; interaction, P=0.2; n=50 for all points).

To quantify the benefit of Mauthner cell recruitment at different times to intercept, we calculated the percent change in the proportion of the motor volume not engulfed from Mauthner-silent to Mauthner-active volumes (Fig. 7G). Our simulations showed that Mauthner activation increased the proportion of the fish motor volume not engulfed by the mask by 30–100% on average for times to intercept of 15–25 ms. Times to intercept longer than 40 ms showed a reduced benefit of Mauthner cell recruitment since slower escapes would be equally effective in evading the mask's swept volume. Moreover, times to intercept shorter than 7 ms also had reduced benefit from recruiting the Mauthner cell since that amount of time is inadequate for generating substantial movement.

This analysis demonstrates how simulations of prey motor volume and predator swept volume can be used to estimate the utility of recruiting specialized escape circuits in response to an attack. Moreover, the intersection of these volumes provides insight into how the time to intercept shapes the outcome of the predatory interaction. Also, it may clarify the lack of impact of response latency on escape success, since similar response latency values can be associated with different values of time to intercept after threat response.

DISCUSSION

Our goal was to evaluate how escape maneuver parameters of prey interact to influence survival. By analyzing the escape responses of larval zebrafish to attacks from dragonfly nymphs, we identified the time remaining for the dragonfly mask to reach the fish from the onset of the fish's escape response as most predictive of escape success. We call this parameter the time to intercept after threat response and explain its role in determining the volume of space that contains all possible trajectories of the fish – the fish motor volume. Using a computational approach, we estimated the fish motor volume for different times to intercept to quantify the fish's ability to evade the capture volume of the nymph – the volume swept by the mask. Additionally, we used this approach of analyzing motor volumes to calculate the utility of recruiting the Mauthner neuron for generating the escape by estimating the relative increase in escape success probability.

Journal of Experimental Biology (2021) 224, jeb235481. doi:10.1242/jeb.235481

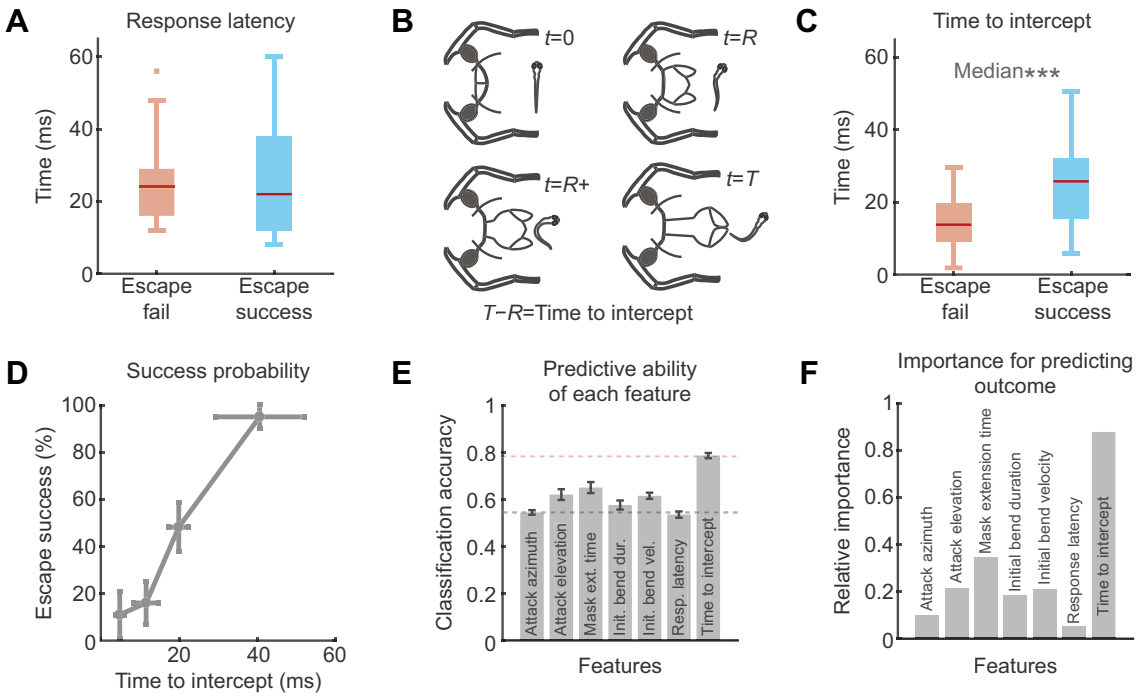

Fig. 6. Importance of time to intercept. (A) There is no significant difference between response latencies of failed and successful fish escapes. Red line of box-and-whisker is median, box extends from 25th to 75th percentiles, and whiskers extend to the most extreme data points not considered outliers. (B) The time to intercept after threat response is the time at the start of the fish escape response (*t*=*R*) subtracted from the mask extension time (*t*=*T*). (C) The time to intercept is significantly longer for successful escapes than for failed escapes. Box-and-whisker details as in A. (D) Escape success probability as a function of time to intercept binned into quartiles (mean±s.d. for *x*- and *y*-axes). Escape success probability increases with time to intercept. (E) Classification accuracy (mean±s.e.m.) of random forest classifiers in predicting escape outcome when trained on only one parameter with 10-fold cross validation. The gray dashed line is the naive classification accuracy of 0.55 and the pink dashed line at 0.79 is classification accuracy of a random forest classifier trained on all of the parameters to predict the escape outcome. The classifier using only time to intercept after threat response significantly outperformed classifiers trained on any of the other parameters and is not significantly different from a classifier trained on all of the parameters together. (F) The relative importance of parameters in a random forest classifier trained to predict escape outcomes using all parameters. Time to intercept after threat response is dramatically more important than other parameters. ***P<0.001

We argue that the time to intercept robustly determines the outcome since it defines the fish motor volume (Snyder et al., 2007). This perspective can clarify the influence of response latency, speed, and direction of an escape maneuver on evasion success across different predation contexts. For the same time to intercept, faster escape speeds would increase the size of the fish motor volume and therefore increase the proportion of the motor volume not engulfed by the capture volume of the predator. This explains the existing evidence in support of the benefit of fast speeds during escape (Webb, 1986; Walker et al., 2005). However, escape responses to slower predators that allow for more time to intercept may not require the fastest speeds for successful evasion, as evidenced by findings in other studies (Fuiman et al., 2006; Soto et al., 2015; Nair et al., 2015).

Shorter escape response latencies for the same strike would increase the time to intercept, the fish motor volume, and thus, the non-engulfed fraction. Unexpectedly, we find that the response latency of larval fish was not significantly different for failed and successful escapes. We ascribe this to the variability of dragonfly mask extension times (Fig. 6D) where the same fish response latency can produce a successful escape in the case of a longer extension time and a failed escape for a shorter one. However, when the duration of predatory strikes is more consistent, changes in escape latency would produce changes in evasion success, as seen in other studies (Fuiman et al., 2006; Stewart et al., 2013; Nair et al., 2017; McCormick et al., 2018).

The response latency of the prey is also related to the distance at which it can sense the predator. Sensing range was found to be critical to evasion success in some studies (Nair et al., 2017; Free et al., 2019). While this parameter may be more relevant to pursuit predation, it can still be understood within the framework of motor volumes and the time to intercept after threat response. Clearly, with longer sensing range, the prey is afforded more time to intercept, increasing its motor volume and chances of surviving. However, escaping earlier allows the predator opportunity to change course and follow suit. In these scenarios, the prey may wait to initiate an evasive maneuver even after sensing the predator, to outmaneuver it at closer distances (Wilson et al., 2018) where the motor volume of the stopped prey is less directionally biased than that of the fast-moving predator.

Finally, specific escape directions that lead the prey out of the capture volume of a predator also lead to successful escapes. For longer times to intercept, we found that a number of directions in the nearly spherical motor volume of the fish led out of the capture volume. Similarly, others have shown that successful escape trajectories are not required to follow a single optimal trajectory (Domenici et al., 2011a,b) and can even be directed towards the attack (Corcoran and Conner, 2016). However, scenarios where the predator capture volume engulfs a large portion of the prey motor volume would leave only a subset of directions that successfully evade the attack. For such cases, the appropriate choice of escape direction would be vital to survival, as shown in modeling studies (Howland, 1974; Weihs and Webb, 1984) and behavioral experiments (Kimura and Kawabata, 2018). In our data, when the mask engulfed a large portion of the fish motor volume, fish had low survival rates, possibly because their escapes were not directed away from the attacks.

Journal of Experimental Biology (2021) 224, jeb235481. doi:10.1242/jeb.235481

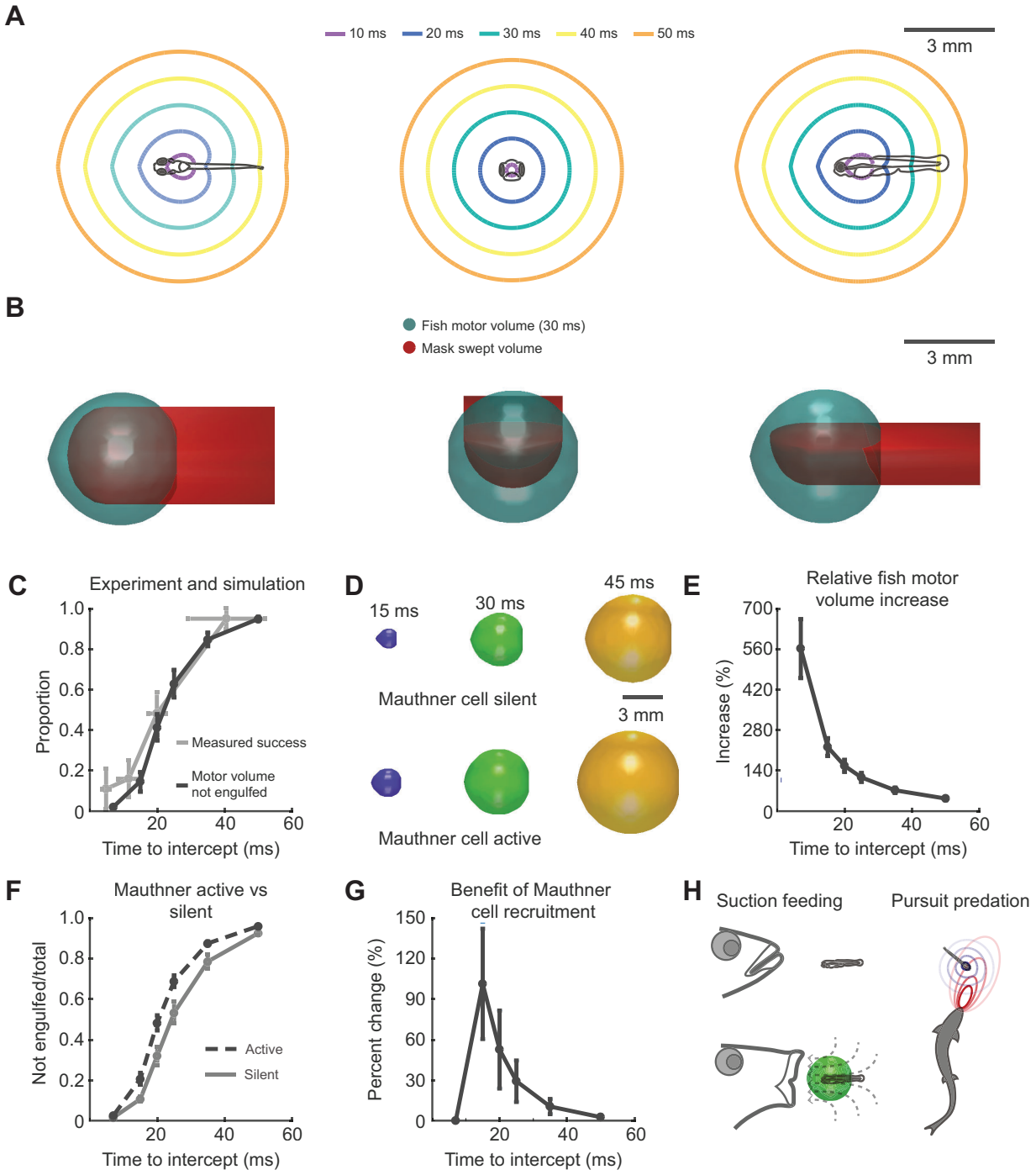

Fig. 7. Fish motor volume at the time to intercept. (A) Top, front and side view cross sections of surface isochrones of the larval zebrafish motor volume for times within the range of values for time to intercept. (B) Top, front and side view perspectives visualizing the intersection of the mask swept volume with the larval zebrafish motor volume for the time to intercept of 30 ms. (C) The darker line represents the proportion of the larval zebrafish motor volume not engulfed by the mask swept volume for different values of time to intercept (mean±s.d.). The lighter line represents the proportion of successful escape responses as a function of time to intercept binned into quartiles (mean±s.d.). The non-engulfed fraction of the motor volume increases with time to intercept. There is no significant difference between the proportion of the motor volume not engulfed and the proportion of successful escape responses. (D) Visualization of the estimated larval zebrafish motor volume at different times to intercept for the Mauthner-silent and Mauthner-active responses. The initial bend velocity used to generate the motor volumes were different for Mauthner cell silent and active responses but the same propulsive velocity was used for both (see Materials and Methods). (E) The relative increase in motor volume for different values of time to intercept when comparing Mauthner-silent to Mauthner-active volumes (mean±s.e.m.). The increase in volume is greatest for shorter values of time to intercept. (F) The proportion of the larval zebrafish motor volume not engulfed by the mask swept volume for different values of time to intercept for Mauthner silent and active responses (mean±s.d.). There is a significant difference in the proportion of the fish motor volume not engulfed for Mauthner active responses. (G) The percent change in the proportion of the fish motor volume not engulfed when comparing Mauthner silent to active responses. The most dramatic increases are seen for mid-range values of time to intercept. (H) Suction feeding: larval fish motor volume and predator ingested volume interaction during suction feeding. The ingested volume is similar to mask capture volume. Pursuit predation: predator and prey motor volume interaction during pursuit predation.

The lack of correlation between the attack direction and escape direction aligns with existing findings of larval zebrafish escapes initiated by flow sensing (Stewart et al., 2014). However, others have shown that adult goldfish and angelfish can direct escapes away from flow and mechanosensory stimuli (Eaton and Emberley, 1991; Domenici and Blake, 1993). This difference between adult and larval fish may be because the larger body of the adults affords a clearer distinction of flow speed differences across the body to guide directional escapes, especially in more turbulent flow structures.

Different predatory scenarios may change the relative importance of response latency, speed, direction or even other parameters in producing successful escapes. However, here we unify the influence of these parameters on the escape outcome by clarifying their role in generating the critical non-overlapping regions of the predator and prey volumes.

We found that escapes were initiated in response to the flow stimulus of the mask extension. Notably, faster fluid velocities due to mask movement produced shorter latency escape responses, with faster initial bends and shorter initial bend durations. These escape kinematics suggest that fish were more likely to recruit the Mauthner cell in response to higher magnitude perturbations. The argument for differential Mauthner cell recruitment based on stimulus parameters is well supported by previous findings which show that fish perform a graded assessment of threat (Bhattacharyya et al., 2017).

Furthermore, our simulations showed that Mauthner activation dramatically increased the proportion of the fish motor volume not engulfed by the mask for a specific range of times to intercept from 15 to 25 ms. Since this range composes a significant proportion of the observed range of times to intercept, there is a clear functional benefit of recruiting the Mauthner neuron in this predatory context, also now demonstrated experimentally (Hecker et al., 2020).

However, our simulations also suggested a reduced benefit from recruiting the Mauthner cell for larger values of time to intercept because motor networks producing slower movements would be equally effective. This result aligns with existing findings which demonstrate that fish are less likely to deploy a Mauthner active escape in response to slower approaching predators (Eaton et al., 1984; Bhattacharyya et al., 2017). Surprisingly, there was also reduced benefit from recruiting the Mauthner cell for very small values of time to intercept since there is no possibility of escaping the capture volume. This potentially explains freezing behavior in cases where sensory information reports there is not enough time to escape (Chelini et al., 2009; Egan et al., 2009; Herberholz and Marquart, 2012; Bhattacharyya et al., 2017).

Our results extend directly to aquatic suction feeding (Fig. 7H) since the volume ingested by the predator is analogous to the mask swept volume. In support, other researchers have demonstrated that the accuracy of aiming during suction feeding is critical in determining the outcome of the strike (Kane and Higham, 2014). Poorly aimed ingested volumes would overlap less with the prey motor volume, leaving regions of safety for the prey. The prevalence of suction feeding in a variety of fish (Wainwright et al., 2007) indicates that the framework presented here fits an array of aquatic predatory interactions.

For prey, the time to intercept is related to the speed of the predatory attack at the moment the attack is sensed. Though it is unclear whether animals estimate this parameter for flow stimuli, studies suggest that animals do estimate the time remaining to capture for looming visual stimuli (Rind and Simmons, 1999; Santer et al., 2006; Liu et al., 2011). Conceivably, faster attacks that produce more intense sensory stimuli push the estimates of time to intercept to lower values. These estimates of time to intercept directly correspond to the utility of deploying different escape maneuvers. This aligns with existing evidence of more intense stimuli producing shorter latency and higher speed escape responses in other animals (Edwards et al., 1999; von Reyn et al., 2014). Given the importance of time to intercept in predicting the escape outcome, the evidence that prey estimate this parameter, and its ability to determine the utility of different escape responses, we expect that the time to intercept after threat response is under significant selection pressure. The stage is now set for using the larval zebrafish model system to understand how the computation of the time to intercept may be implemented by the nervous system.

More generally, predator and prey motor volumes provide a method to compare the maneuverability of each agent through the predatory interaction. This also applies to pursuit predation (Fig. 7H), where the motor volumes change over time as predator and prey attempt to outrun and out-maneuver each other (Moore and Biewener, 2015; Wilson et al., 2018). The regions of the prey motor volume not intersecting with the predator engulfing volume denote the subset of movements and corresponding neural circuits that constitute successful evasive strategies. This subset has clear implications for decision-making during escape and the evolutionary pressure on the selection of appropriate maneuvers to increase survival. The approach presented here provides a method to estimate the utility of specific escape maneuvers by connecting the interplay of many temporal and kinematic parameters to their influence in shaping the reachable spaces of predator and prey.

Acknowledgements
We thank Neelesh Pantankar for his guidance with fluid mechanics. Additionally, we acknowledge members of the McLean lab for their advice in experimental protocols and Elissa Szuter for technical help maintaining the fish colony.

Competing interests
The authors declare no competing or financial interests.

Author contributions
Conceptualization: K.B., D.L.M., M.A.M.; Methodology: K.B., D.L.M., M.A.M.; Software: K.B.; Formal analysis: K.B.; Writing - original draft: K.B., D.L.M., M.A.M.; Writing - review & editing: K.B., D.L.M., M.A.M.; Visualization: K.B., D.L.M., M.A.M.; Supervision: D.L.M., M.A.M.; Project administration: D.L.M., M.A.M.; Funding acquisition: D.L.M., M.A.M.

Funding
This work was supported by the National Science Foundation (NSF-IOS 1456830, NSF-ECCS 1835389) and National Institutes of Health (R01-NS067299). Deposited in PMC for release after 12 months.

Supplementary information
Supplementary information available online at
https://jeb.biologists.org/lookup/doi/10.1242/jeb.235481.supplemental

References
Bhattacharyya, K., McLean, D. L. and MacIver, M. A. (2017). Visual threat assessment and reticulospinal encoding of calibrated responses in larval zebrafish. *Curr. Biol.* **27**, 2751-2762. doi:10.1016/j.cub.2017.08.012

Bhattacharyya, K., McLean, D. L. and MacIver, M. A. (2020). MacIver-Lab/IntersectionOfMotorVolumes: Code for "Intersection of motor volumes predicts the outcome of ambush predation of larval zebrafish". https://doi.org/10.5281/zenodo.4245588.

Blanke, A., Busse, S. and Machida, R. (2015). Coding characters from different life stages for phylogenetic reconstruction: a case study on dragonfly adults and larvae, including a description of the larval head anatomy of *Epiophlebia superstes* (Odonata: Epiophlebiidae). *Zool. J. Linn. Soc.* **174**, 718-732. doi:10.1111/zoj.12258

Breiman, L. (2001). Random forests. *Mach. Learn.* **45**, 5-32. doi:10.1023/A:1010933404324

Budick, S. A. and O'Malley, D. M. (2000). Locomotor repertoire of the larval zebrafish: swimming, turning and prey capture. *J. Exp. Biol.* **203**, 2565-2579.

Burgess, H. A. and Granato, M. (2007). Sensorimotor gating in larval zebrafish. *J. Neurosci.* **27**, 4984-4994. doi:10.1523/JNEUROSCI.0615-07.2007

Busse, S. and Gorb, S. N. (2018). Material composition of the mouthpart cuticle in a damselfly larva (Insecta: Odonata) and its biomechanical significance. *R. Soc. Open Sci.* **5**. doi:10.1098/rsos.172117
Card, G. M. (2012). Escape behaviors in insects. *Curr. Opin. Neurobiol.* **22**, 180-186. doi:10.1016/j.conb.2011.12.009
Chelini, M. C., Willemart, R. H. and Hebets, E. A. (2009). Costs and benefits of freezing behaviour in the harvestman *Eumesosoma roeweri* (Arachnida, Opiliones). *Behav. Processes* **82**, 153-159. doi:10.1016/j.beproc.2009.06.001
Corcoran, A. J. and Conner, W. E. (2016). How moths escape bats: predicting outcomes of predator–prey interactions. *J. Exp. Biol.* **219**, 2704-2715. doi:10.1242/jeb.137638
Dangles, O., Ory, N., Steinmann, T., Christides, J. P. and Casas, J. (2006). Spider's attack versus cricket's escape: velocity modes determine success. *Anim. Behav.* **72**, 603-610. doi:10.1016/j.anbehav.2005.11.018
deVries, M. S., Murphy, E. A. K. and Patek, S. N. (2012). Strike mechanics of an ambush predator: the spearing mantis shrimp. *J. Exp. Biol.* **215**, 4374-4384. doi:10.1242/jeb.075317
DiDomenico, R. and Eaton, R. C. (1988). Seven principles for command and the neural causation of behavior. *Brain Behav. Evol.* **31**, 125-140. doi:10.1159/000116580
DiDomenico, R., Nissanov, J. and Eaton, R. C. (1988). Lateralization and adaptation of a continuously variable behavior following lesions of a reticulospinal command neuron. *Brain Res.* **473**, 15-28. doi:10.1016/0006-8993(88)90310-1
Domenici, P. (2002). The visually mediated escape response in fish: Predicting prey responsiveness and the locomotor behaviour of predators and prey. *Mar. Freshw. Behav. Physiol.* **35**, 87-110. doi:10.1080/10236240290025635
Domenici, P. (2010). Context-dependent variability in the components of fish escape response: integrating locomotor performance and behavior. *J. Exp. Zool. A Ecol. Genet. Physiol.* **313**, 59-79. doi:10.1002/jez.580
Domenici, P. and Blake, R. W. (1993). Escape trajectories in angelfish (*Pterophyllum eimekei*). *J. Exp. Biol* **177**, 253-272.
Domenici, P., Blagburn, J. M. and Bacon, J. P. (2011a). Animal escapology I: theoretical issues and emerging trends in escape trajectories. *J. Exp. Biol.* **214**, 2463-2473. doi:10.1242/jeb.029652
Domenici, P., Blagburn, J. M. and Bacon, J. P. (2011b). Animal escapology II: escape trajectory case studies. *J. Exp. Biol.* **214**, 2474-2494. doi:10.1242/jeb.053801
Driver, P. M. and Humphries, D. A. (1970). Protean displays as inducers of conflict. *Nature* **226**, 968-969. doi:10.1038/226968a0
Dunn, T. W., Gebhardt, C., Naumann, E. A., Riegler, C., Ahrens, M. B., Engert, F. and Del Bene, F. (2016). Neural circuits underlying visually evoked escapes in larval zebrafish. *Neuron* **89**, 613-628. doi:10.1016/j.neuron.2015.12.021
Eaton, R. C. and Emberley, D. S. (1991). How stimulus direction determines the trajectory of the Mauthner-initiated escape response in a teleost fish. *J. Exp. Biol.* **161**, 469-487.
Eaton, R. C., Nissanov, J. and Wieland, C. M. (1984). Differential activation of Mauthner and non-Mauthner startle circuits in the zebrafish: implications for functional substitution. *J. Comp. Physiol. A* **155**, 813-820. doi:10.1007/BF00611598
Eaton, R. C., DiDomenico, R. and Nissanov, J. (1991). Role of the Mauthner cell in sensorimotor integration by the brain stem escape network. *Brain Behav. Evol.* **37**, 272-285. doi:10.1159/000114365
Eaton, R. C., Hofve, J. C. and Fetcho, J. R. (1995). Beating the competition: the reliability hypothesis for Mauthner axon size. *Brain Behav. Evol.* **45**, 183-194. doi:10.1159/000113549
Edut, S. and Eilam, D. (2004). Protean behavior under barn-owl attack: voles alternate between freezing and fleeing and spiny mice flee in alternating patterns. *Behav. Brain Res.* **155**, 207-216. doi:10.1016/j.bbr.2004.04.018
Edwards, D. H., Heitler, W. J. and Krasne, F. B. (1999). Fifty years of a command neuron: the neurobiology of escape behavior in the crayfish. *Trends Neurosci.* **22**, 153-161. doi:10.1016/S0166-2236(98)01340-X
Egan, R. J., Bergner, C. L., Hart, P. C., Cachat, J. M., Canavello, P. R., Elegante, M. F., Elkhayat, S. I., Bartels, B. K., Tien, A. K., Tien, D. H. et al. (2009). Understanding behavioral and physiological phenotypes of stress and anxiety in zebrafish. *Behav. Brain Res.* **205**, 38-44. doi:10.1016/j.bbr.2009.06.022
Engeszer, R. E., Patterson, L. B., Rao, A. A. Parichy, D. M. (2007). Zebrafish in the wild: A review of natural history and new notes from the field. *Zebrafish* **4**, 21-40. doi:10.1089/zeb.2006.9997
Fitzpatrick, R. (2017). *Theoretical Fluid Mechanics*. IOP Publishing.
Free, B. A., McHenry, M. J. and Paley, D. A. (2019). Probabilistic analytical modelling of predator–prey interactions in fishes. *J. R. Soc. Interface* **16**, 20180873. doi:10.1098/rsif.2018.0873
Friedman, J. H., Bentley, J. L. and Finkel, R. A. (1977). An algorithm for finding best matches in logarithmic expected time. *ACM Trans. Math. Softw.* **3**, s209-s226. doi:10.1145/355744.355745
Fuiman, L. A., Rose, K. A., Cowan, J. H. and Smith, E. P. (2006). Survival skills required for predator evasion by fish larvae and their relation to laboratory measures of performance. *Anim. Behav.* **71**, 1389-1399. doi:10.1016/j.anbehav.2005.11.013
Hale, M. E., Katz, H. R., Peek, M. Y. and Fremont, R. T. (2016). Neural circuits that drive startle behavior, with a focus on the Mauthner cells and spiral fiber neurons of fishes. *J. Neurogenet.* **30**, 89-100. doi:10.1080/01677063.2016.1182526
Harris, J. A., Cheng, A. G., Cunningham, L. L., MacDonald, G., Raible, D. W. and Rubel, E. W. (2003). Neomycin-induced hair cell death and rapid regeneration in the lateral line of zebrafish (*Danio rerio*). *J. Assoc. Res. Otolaryngol.* **4**, 219-234. doi:10.1007/s10162-002-3022-x
Hecker, A., Schulze, W., Oster, J., Richter, D. O. and Schuster, S. (2020). Removing a single neuron in a vertebrate brain forever abolishes an essential behavior. *Proc. Natl Acad. Sci. USA* **117**, 3254-3260. doi:10.1073/pnas.1918578117
Herberholz, J. and Marquart, G. D. (2012). Decision making and behavioral choice during predator avoidance. *Front. Neurosci.* **6**, 125. doi:10.3389/fnins.2012.00125
Howland, H. C. (1974). Optimal strategies for predator avoidance - relative importance of speed and maneuverability. *J. Theor. Biol.* **47**, 333-350. doi:10.1016/0022-5193(74)90202-1
Kane, E. A. and Higham, T. E. (2014). Modelled three-dimensional suction accuracy predicts prey capture success in three species of centrarchid fishes. *J. R. Soc. Interface* **11**, 20140223. doi:10.1098/rsif.2014.0223
Katzir, G. (1993). Escape response of black mollies (*Poecilia shenops*) to predatory dives of a pied kingfisher (Ceryle rudis). *Copeia* **1993**, 549-553. doi:10.2307/1447160
Kimura, H. and Kawabata, Y. (2018). Effect of initial body orientation on escape probability of prey fish escaping from predators. *Biol. Open* **7**, bio023812. doi:10.1242/bio.023812
Kohashi, T. and Oda, Y. (2008). Initiation of Mauthner- or non-Mauthner-mediated fast escape evoked by different modes of sensory input. *J. Neurosci.* **28**, 10641-10653. doi:10.1523/JNEUROSCI.1435-08.2008
Korn, H. and Faber, D. S. (2005). The Mauthner cell half a century later: a neurobiological model for decision-making? *Neuron* **47**, 13-28. doi:10.1016/j.neuron.2005.05.019
Lin, H.-T. and Leonardo, A. (2017). Heuristic rules underlying dragonfly prey selection and interception. *Curr. Biol.* **27**, 1124-1137. doi:10.1016/j.cub.2017.03.010
Liu, K. S. and Fetcho, J. R. (1999). Laser ablations reveal functional relationships of segmental hindbrain neurons in zebrafish. *Neuron* **23**, 325-335. doi:10.1016/S0896-6273(00)80783-7
Liu, Y. J., Wang, Q. and Li, B. (2011). Neuronal responses to looming objects in the superior colliculus of the cat. *Brain Behav. Evol.* **77**, 193-205. doi:10.1159/000327045
McCormick, M. I., Fakan, E. and Allan, B. J. M. (2018). Behavioural measures determine survivorship within the hierarchy of whole-organism phenotypic traits. *Funct. Ecol.* **32**, 958-969. doi:10.1111/1365-2435.13033
McHenry, M. J., Feitl, K. E., Strother, J. A. and Van Trump, W. J. (2009). Larval zebrafish rapidly sense the water flow of a predator's strike. *Biol. Lett.* **5**, 477-479. doi:10.1098/rsbl.2009.0048
Mischiati, M., Lin, H.-T., Herold, P., Imler, E., Olberg, R. and Leonardo, A. (2015). Internal models direct dragonfly interception steering. *Nature* **517**, 333-338. doi:10.1038/nature14045
Moore, T. Y. and Biewener, A. A. (2015). Outrun or outmaneuver: Predator-prey interactions as a model system for integrating biomechanical studies in a broader ecological and evolutionary context. *Integr. Comp. Biol.* **55**, 1188-1197. doi:10.1093/icb/icv074
Nair, A., Azatian, G. and McHenry, M. J. (2015). The kinematics of directional control in the fast start of zebrafish larvae. *J. Exp. Biol.* **218**, 3996-4004. doi:10.1242/jeb.126292
Nair, A., Nguyen, C. and McHenry, M. J. (2017). A faster escape does not enhance survival in zebrafish larvae. *Proc. Biol. Sci.* **284**. doi:10.1098/rspb.2017.0359
Neki, D., Nakayama, H., Fujii, T., Matsui-Furusho, H. and Oda, Y. (2014). Functional motifs composed of morphologically homologous neurons repeated in the hindbrain segments. *J. Neurosci.* **34**, 3291-3302. doi:10.1523/JNEUROSCI.4610-13.2014
Nissanov, J., Eaton, R. C. and DiDomenico, R. (1990). The motor output of the Mauthner cell, a reticulospinal command neuron. *Brain Res.* **517**, 88-98. doi:10.1016/0006-8993(90)91012-6
O'Malley, D. M., Kao, Y. H. and Fetcho, J. R. (1996). Imaging the functional organization of zebrafish hindbrain segments during escape behaviors. *Neuron* **17**, 1145-1155. doi:10.1016/S0896-6273(00)80246-9
Olesen, J. (1972). The hydraulic mechanism of labial extension and jet propulsion in dragonfly nymphs. *J. Comp. Physiol.* **81**, 53. doi:10.1007/BF00693549
Olesen, J. (1978). Prey capture in dragonfly nymphs (Odonata, Insecta): Labial protraction by means of a multi-purpose abdominal pump. *Videnskabelige Meddelelser fra dansk naturhistorisk Forening*, Vidensk. Meddr dansk naturh. Foren., 06.
Parry, D. A. (1983). Labial extension in the dragonfly larva *Anax imperator*. *J. Exp. Biol.* **107**.
Pritchard, G. (1965). Prey capture by dragonfly larvae (Odonata; Anisoptera). *Can. J. Zool.* **43**, 271. doi:10.1139/z65-026
Rind, F. C. and Simmons, P. J. (1999). Seeing what is coming: building collision-sensitive neurones. *Trends Neurosci.* **22**, 215-220. doi:10.1016/S0166-2236(98)01332-0

Robert Evans Snodgrass (1954). *The Dragonfly Larva: Smithsonian Miscellaneous Collections*. Washington: Smithsonian Institution.
Santer, R. D., Rind, F. C., Stafford, R. and Simmons, P. J. (2006). Role of an identified looming-sensitive neuron in triggering a flying locust's escape. *J. Neurosphysiol.* **95**, 3391-3400. doi:10.1152/jn.00024.2006
Sillar, K. T., Picton, L. D. and Heitler, W. J. (2016). *The Neuroethology of Predation and Escape*. Wiley.
Snyder, J. B., Nelson, M. E., Burdick, J. W. and MacIver, M. A. (2007). Omnidirectional sensory and motor volumes in an electric fish. *PLoS Biol.* **5**, 2671-2683. doi:10.1371/journal.pbio.0050301
Soto, A., Stewart, W. J. and McHenry, M. J. (2015). When optimal strategy matters to prey fish. *Integr. Compar. Biol.* **55**, 110-120. doi:10.1093/icb/icv027
Sperling, E. A., Frieder, C. A., Raman, A. V., Girguis, P. R., Levin, L. A. and Knoll, A. H. (2013). Oxygen, ecology, and the Cambrian radiation of animals. *Proc. Natl. Acad. Sci. USA* **110**, 13446-13451. doi:10.1073/pnas.1312778110
Stewart, W. J., Cardenas, G. S. and McHenry, M. J. (2013). Zebrafish larvae evade predators by sensing water flow. *J. Exp. Biol.* **216**, 388-398. doi:10.1242/jeb.072751
Stewart, W. J., Nair, A., Jiang, H. and McHenry, M. J. (2014). Prey fish escape by sensing the bow wave of a predator. *J. Exp. Biol.* **217**, 4328-4336. doi:10.1242/jeb.111773
Tanaka, Y. and Hisada, M. (1980). The hydraulic mechanism of the predatory strike in dragonfly larvae. *J. Exp. Biol.* **88**.
von Reyn, C. R., Breads, P., Peek, M. Y., Zheng, G. Z., Williamson, W. R., Yee, A. L., Leonardo, A. and Card, G. M. (2014). A spike-timing mechanism for action selection. *Nat. Neurosci.* **17**, 962-970. doi:10.1038/nn.3741
Wainwright, P., Carroll, A. M., Collar, D. C., Day, S. W., Higham, T. E. and Holzman, R. A. (2007). Suction feeding mechanics, performance, and diversity in fishes. *Integr. Comp. Biol.* **47**, 96-106. doi:10.1093/icb/icm032
Walker, J. A., Ghalambor, C. K., Griset, O. L., McKenney, D. and Reznick, D. N. (2005). Do faster starts increase the probability of evading predators? *Funct. Ecol.* **19**, 808-815. doi:10.1111/j.1365-2435.2005.01033.x
Webb, P. W. (1986). Effect of body form and response threshold on the vulnerability of four species of teleost prey attacked by largemouth bass (*Micropterus salmoides*). *Can. J. Fish. Aquat. Sci.* **43**, 763-771. doi:10.1139/f86-094
Weihs, D. and Webb, P. W. (1984). Optimal avoidance and evasion tactics in predator-prey interactions. *J. Theor. Biol.* **106**, 189-206. doi:10.1016/0022-5193(84)90019-5
Wilson, A. M., Hubel, T. Y., Wilshin, S. D., Lowe, J. C., Lorenc, M., Dewhirst, O. P., Bartlam-Brooks, H. L. A., Diack, R., Bennitt, E., Golabek, K. A. et al. (2018). Biomechanics of predator–prey arms race in lion, zebra, cheetah and impala. *Nature* **554**, 183-188. doi:10.1038/nature25479